Nanoscale Volcanoes: Accretion of Matter at Ion-Sculpted Nanopores

Nanoscale Volcanoes: Accretion of Matter at Ion-Sculpted Nanopores

Toshiyuki Mitsui, Derek Stein, Young-Rok Kim, David Hoogerheide, and J. A. Golovchenko
Harvard University, Cambridge, Massachusetts 02138, USA
(Received 5 May 2005; published 23 January 2006)

We demonstrate the formation of nanoscale volcanolike structures induced by ion-beam irradiation of nanoscale pores in freestanding silicon nitride membranes. Accreted matter is delivered to the volcanoes from micrometer distances along the surface. Volcano formation accompanies nanopore shrinking and depends on geometrical factors and the presence of a conducting layer on the membrane's back surface. We argue that surface electric fields play an important role in accounting for the experimental observations.

DOI: 10.1103/PhysRevLett.96.036102 PACS numbers: 81.07.De, 81.16.Rf, 81.40.Wx

Single nanopores with diameters less than 2 nm have recently been fabricated in thin, insulating solid-state membranes using a method called ion-beam sculpting [1]. In aqueous solutions, these nanopores function as single molecule detectors that electronically measure the length and folding conformation of DNA molecules passing through the nanopore [2,3]. These nanopores may play a significant role in molecular electronics and rapid DNA sequencing strategies. Notwithstanding the large body of existing knowledge involving ion-beam-induced sputter erosion, atomic displacements, implantation, surface diffusion, and viscous flow [4–15], the mechanism responsible for the formation of these extremely small nanopores is still obscure. In this Letter, we present several unanticipated phenomena that provide new insight into the physical mechanisms involved.

In Ref. [1], ion-beam-induced pore closing was measured *in situ* by monitoring ions transmitted through the pore into a detector, as depicted in Figs. 1(a) and 1(b), and was confirmed by TEM imaging. A surface diffusion model was posited where the incident ion beam (3 keV Ar^+) creates mobile surface atoms that diffuse to and close the pore. A net flow of atoms to the pore was subsumed in a mathematical boundary condition of zero mobile surface atom concentration at the moving pore boundary, where the delivered atoms shrink the pore. Fitting the model to the observed pore closing rate implied that mobile surface atoms were delivered to the pore from as far as 50 nm away. Here we perform atomic force microscope (AFM) studies of the surface region near ion-sculpted nanopores, revealing that much more matter accumulates near the nanopore and from much further away than had previously been thought. Evidence is presented that electrical charging of the surface is important in the process.

Samples were fashioned from 0.25 μm thick, low stress $Si_{3.5}N_4$ grown on silicon substrates by chemical vapor deposition. The stoichiometry of the silicon nitride membrane was verified using Rutherford backscattering. A freestanding 30 μm square window of $Si_{3.5}N_4$ was fabricated by lithographically patterning and subsequently etching the silicon substrate below the membrane. A starting pore ~100 nm across was then drilled through the freestanding membrane window at its center with a scanned 50 keV, 10 nm diameter, gallium ion beam from an FEI 9500 focused ion-beam machine (FIB). AFM images show that the pore size at the membrane surface facing the FIB beam was always larger than the pore size on the opposite side, indicating that a truncated conical pore passes through the membrane with a full apex angle of ~10 degrees.

This FIB pore was then closed by exposure to a 300 μm diameter, 3 keV Ar^+ ion beam in an ion-beam sculpting apparatus [16]. The beam was centered on the membrane window and programmed to irradiate with a duty cycle of 100 ms during each second [17]. The ions transmitted through the pore were monitored with a channeltron single-ion counting detector, as illustrated schematically in Fig. 1(a). The argon ion beam was incident on the sample such that the walls of the pore make an acute angle with the Ar^+-irradiated surface.

Figure 1(b) shows the transmitted ion current with increasing beam exposure. The closing pore increasingly blocks the incident beam until finally no ions are trans-

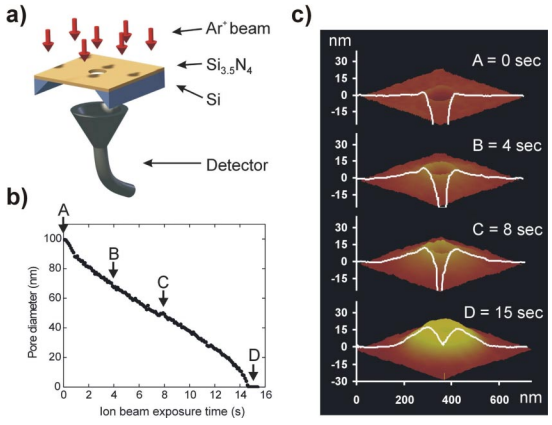

FIG. 1 (color). (a) Schematic of ion-beam sculpting experiment. (b) Nanopore closing curve. (c) AFM surface scans after 0, 4, 8, and 15 s beam exposures.

mitted when the pore is completely closed. The flux was 4.4 Ar^+ per nm^2/ sec during the duty cycle "on time." Pore closing is confirmed by TEM observations.

At exposure times of 0, 4, 8, and 15 s on the closing curve in Fig. 1(b), the sample was imaged *ex situ* in a Digital Instruments (Model 100) AFM equipped with a high resolution "Stinger" silicon tip [18]. Figure 1(c) contains AFM images of the nanopore region for each of the above exposure times, each with a calibrated surface elevation line scan passing across the pore. Clearly observable are "volcanolike" ridge structures that keep growing until the pore has closed. They extend ~100–200 nm from the pore and have elevations up to 15–25 nm above the sputter-eroded flat surface far from the pore. These observations indicate that significantly more material has aggregated in the vicinity of the pore than has previously been assumed or observed. The height of the tallest volcano extends ~10–20 nm past the original presputtered surface height. Volcanolike structures are not observed on the unexposed back surface of the membrane.

Pores formed with the Ar^+ ion beam incident on the same side as the FIB drilling beam, where the walls of the pore form an obtuse angle with the argon-exposed surface, also close but show no volcanolike structure above the flat nitride surface facing the Ar^+ beam. These pores, however, do show an accumulation of matter within the pore (between the front and back surfaces) near its back surface when interrogated with the AFM.

Figure 2 further demonstrates this angular effect. The sample in the FIB was tilted so the axis of the initial pore made a 20° angle to the membrane surface normal, as in Fig. 2(a). Under these conditions, part of the pore makes an acute angle with the flat surface and part makes an obtuse angle with it. As seen in Fig. 2(b), only the side of the pore with an acute angle to the surface develops the volcanolike ridge.

Experiments were also performed with a 5×5 square array of 100 nm pores centered in the membrane window, spaced 1 μm apart, as shown in Fig. 3(a). The single AFM line scan height plot extends along a diagonal connecting opposite corner pores. Argon beam exposure initially resulted in the corner pores developing the highest volcano structures, the side pores slightly lower structures, and those on the inside increasingly smaller ones as the center pore of the array is approached, as shown in Fig. 3(b). For this image, the sample was exposed to a flux of 4.4 Ar^+ per nm^2 sec for 30 seconds. Figure 4 shows TEM images of this sample. The pores have closed commensurately with the size of the volcanoes formed, with the center pore virtually unclosed, and with the corner pores completely closed [19]. The pores appear to compete for mobile matter over micron distances; the corner pores have the greatest access to the mobile matter and the center pore the least access.

This surprising notion is reinforced by observing the evolution of the nanopore array structure after the outermost pores have completely closed. Figure 3(c) shows

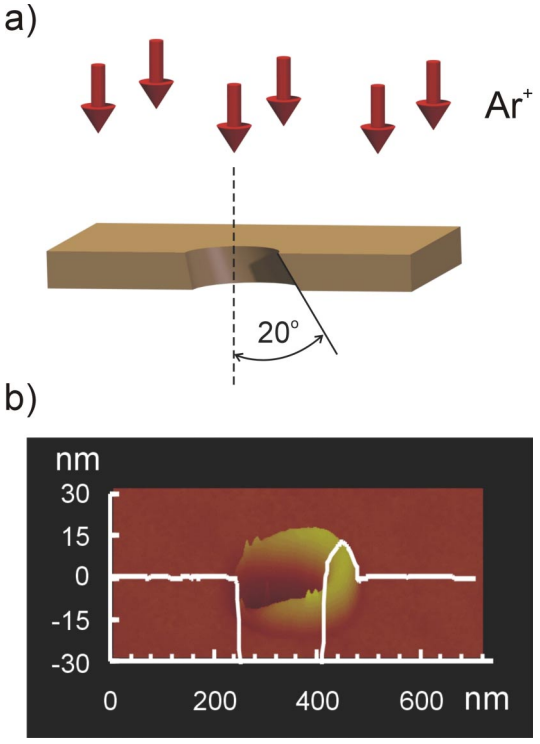

FIG. 2 (color). (a) A pore making a 20° angle to surface. (b) A volcano forms on the acute angle side of the pore.

further evolution of the volcanoes after the corner pores have closed and a second equal ion-beam dose has been applied. Remarkably, volcano structures at the corners diminish in size as those around the side pores grow to their maximum height. The first inside diagonal pore also begins to close and develops a small volcano structure, while the innermost pore still remains unaffected. As shown in Fig. 3(d), another 30 s dose results in a further

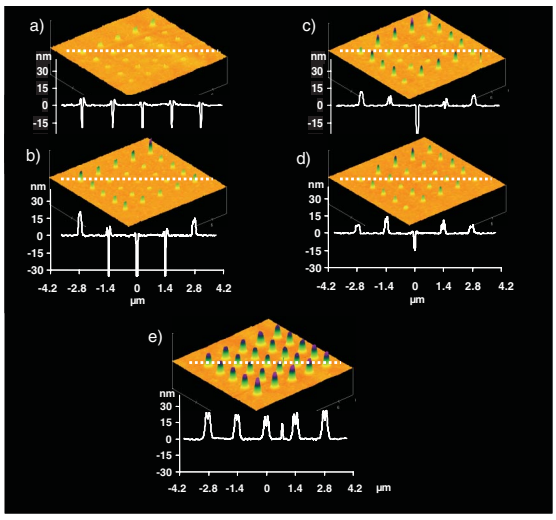

FIG. 3 (color). (a)–(d) Array of pores after successive equal exposures to an Ar^+ ion beam. The original, presputtered level is at ~5 nm, as calculated from the known sputter yield of Ar^+ on silicon nitride. (e) Volcanoes on a gold backed membrane.

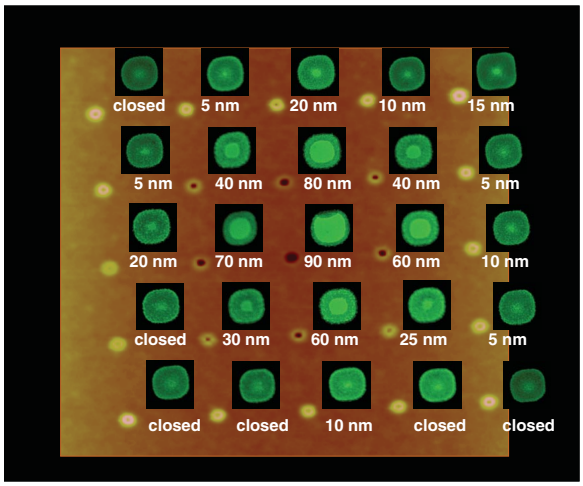

FIG. 4 (color). Individual nanopore TEM images overlaid on the AFM image of the Fig. 3(b) nanopore array.

diminution of the corner pore volcano, while the inner diagonal pores nearly attain their full height, the side pores begin to shrink, and the innermost pore begins to close. The data in Figs. 3(a)–3(d) indicate that the volcanoes develop to a maximum size coincidentally with the closing of the pore, after which they begin to diminish. When they are growing, the volcanoes compete for available matter; the inner pores are almost completely screened from it until the outer pores close.

Figure 3(e) shows the effect of grounding an evaporated conducting layer (50 nm Au on 5 nm Cr) on the backside of the membrane (deposited prior to FIB drilling of the starting pores) during the Ar^+ surface irradiation. The insulating top side of the membrane was exposed to 4.4 Ar^+ per nm^2 sec for 60 s, and it developed a very uniform array of volcanoes. The volcanoes are somewhat higher and broader than those obtained without the conducting back layer. It appears that all pores now have equal access to the supply of mobile matter and that the screening effect has nearly disappeared.

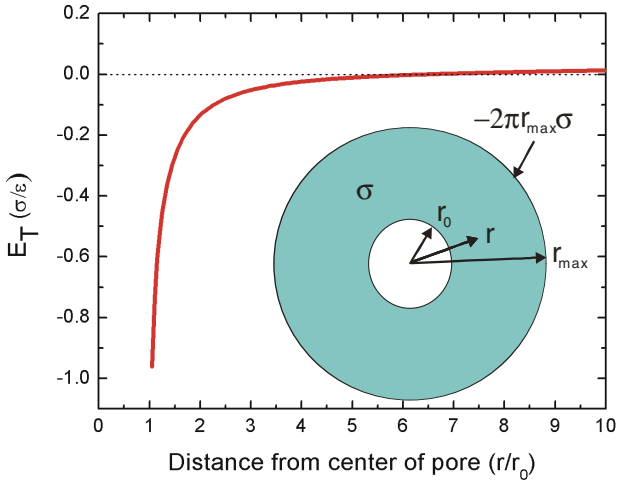

FIG. 5 (color). Plot of in-plane electric field E_T near a nanopore in units of σ/ϵ. Pore radius is at $r/r_0 = 1$.

We postulate that surface electric fields on the ion-beam exposed surface play an important role in volcano formation. Consider the radial in-plane electric field E_T in the surface of a two-dimensional uniform layer of charge of outer radius r_{max} and inner radius r_0. Let there also be a ring of compensating charge at r_{max} that makes the whole structure charge neutral. One then finds E_T as a function of the distance from the pore center, r, to be

$$E_T(r) = -\frac{\sigma}{2\varepsilon}\sum_{m=0}^{\infty}\left(\frac{2m+1}{(m+2)(m-1)} + \frac{m+1}{m+2}\frac{1}{(r/r_0)^{m+2}} - \frac{m}{m-1}\frac{(r/r_0)^{m-1}}{(r_{max}/r_0)^{m-1}}\right)P_m^2(0) + \frac{\sigma}{2\varepsilon} \times \frac{((r_{max}/r_0)^2-1)}{2(r_{max}/r_0)^2}\sum_{m=0}^{\infty} m\frac{(r/r_0)^{m-1}}{(r_{max}/r_0)^{m-1}}P_m^2(0), \quad (1)$$

for $r_0 < r < r_{max}$. Here σ is the surface charge density and the $P_m(x)$ are mth order Legendre polynomials. This result is plotted in units of σ/ϵ and r/r_0 in Fig. 5 for a value of $r_{max}/r_0 = 300$, which approximates our geometry for a 30 μm window, where the nanopore corresponds to the charge-free center disk and the grounded silicon substrate at the edges of the window corresponds to the outer ring of compensating charge. A negative in-plane radial electric field exists for positive σ that attracts positively charged matter towards the pore periphery. It extends over 5.8 r/r_0, the region over which the volcanolike structures grow around the nanopore. For r/r_0 beyond this region, the electric field changes sign and positively charged matter is weakly repelled from the pore. The boundary between these regions increases slowly with r_{max}/r_0.

To estimate the in-plane electric field near the nanopore, we have evaporated gold electrodes on the surface of our samples and observed them to charge up to ~200 volts during ion-beam exposure. This is consistent with the dielectric breakdown voltage of the 0.5 μm silicon nitride dielectric (~10^7 V/cm) [20]. Near the pore, Eq. (1) gives $E_T \sim \sigma/\epsilon = 4 \times 10^6$ V/cm. We posit that such a large field is effective in facilitating both trapping and transport of charged matter along the surface to the pore over distances of several pore radii.

The lack of a noticeable depletion region just outside the volcanoes suggests that surface atoms (not necessarily charged) are constantly being delivered to the pore regions from much further away by ion-beam-induced surface diffusion, where they are captured near the pore by the electric field there. The screening effects observed in Figs. 3(b)–3(d) suggest that this matter, when charged and near the pore, is trapped by the open outer pores in the array before it finds its way to the inner pores. Once a pore closes, it no longer generates an attractive field and stops acting as a trap, allowing inner pores to close. The

data in Fig. 3(b) clearly indicate that the accreted matter arrives from distances greater than 1 μm, which greatly exceeds the 50 nm suggested in Ref. [1].

The fact that pore arrays in membranes backed by a conducting gold layer close more efficiently and more uniformly is consistent with the notion that the mobile surface charge density near the pore is higher on these samples than on a membrane without a conducting backing. The beam-excited surface charged matter likely has a higher sputtering rate due to its repulsion from other positive surface charges. The conducting backing provides an attractive countercharge, which tends to cancel this field-enhanced sputtering effect, enhancing the available charged matter for pore closing. Pore-pore screening effects are thereby mitigated and pore closure rates enhanced. Additional compressive surface normal forces on the ion-beam charged top surface induced by the countercharge in the back electrode may generate local tensile surface forces that further contribute to the accretion of matter near the boundary of the pore.

The observation that volcanolike ridge structures form only on the region of a pore whose wall forms an initially oblique angle with the Ar^+-bombarded surface is compatible with the overall picture presented here. High surface field pointing towards, and terminating at, the top surface pore boundary will be obtained only where the inner pore wall is geometrically blocked from the beam. When the pore's inner wall can be bombarded and charged by the beam, we expect matter to be accreted at the beam boundary inside the pore near the back surface where the electric fields are high, not on the top surface. Indeed, in TEM pictures of ion-sculpted nanopores closed with poorly controlled geometries, we have observed pores to close from different depths and to form overlapping closures from the top and back surfaces.

We conclude by noting that the large mass transport effects reported here with nanopores may be expected whenever preexisting insulating nanostructures are exposed to broad ion beams or when highly focused ion beams are used to form such structures in the first place. Understanding them can result in reliable fabrication of important nanoscale structures. From a more fundamental perspective, it seems clear that modeling studies of ion-induced irradiated nanopore structural transformations can form the basis of a quantitative understanding of surface atom driving forces, transport and accretion. There may also be circumstances in which instabilities such as nanoscale ion-beam-induced surface rippling on insulators [10–14] may be influenced by the surface charging effects and electric fields discussed above. We note that the motion of highly charged matter along a surface may involve collective fluidlike notions as well as those of independent particle diffusion and drift. It will be interesting to see if comprehensive attempts to quantitatively model the transport phenomena and detailed morphological surface evolution presented here can clarify the relative importance of these different approaches to understanding the matter transport involved. Further insight may follow from experimentally determining the elemental content of the accreted matter for different materials. Such measurements on nanometer-sized volcanoes are definitely a challenging experimental problem.

We express our appreciation to Professor L. Hau, Professor D. Branton, and Professor J. Li for valuable discussions. We further acknowledge valuable interactions with members of the Harvard and Agilent Nanopore Groups and support from the DOE and Agilent Technologies.

[1] J. Li *et al.*, Nature (London) **412**, 166 (2001).
[2] J. Li *et al.*, Nat. Mater. **2**, 611 (2003); see also P. Chen *et al.*, Nano Lett. **4**, 2293 (2004).
[3] D. Fologea *et al.*, Nano Lett. **005**, 1905 (2005).
[4] H. Gnaser, *Ion Irradiation of Solid Surfaces* (Springer, Berlin, 1999).
[5] R. E. Johnson and J. Schou, K. Dan. Vidensk. Selsk. Mat. Fys. Medd. **43**, 403 (1993).
[6] P. Sigmund, K. Dan. Vidensk. Selsk. Mat. Fys. Medd. **43**, 7 (1993).
[7] T. Nenadovic *et al.*, Nucl. Instrum. Methods Phys. Res., Sect. B **48**, 538 (1990).
[8] P. G. Snyder *et al.*, Mater. Res. Soc. Symp. Proc. **74**, 535 (1987).
[9] E. A. Eklund *et al.*, Phys. Rev. Lett. **67**, 1759 (1991).
[10] J. Erlebacher *et al.*, Phys. Rev. Lett. **82**, 2330 (1999).
[11] J. Erlebacher, M. J. Aziz, and E. Chason, J. Vac. Sci. Technol. A **18**, 115 (2000).
[12] K Oyoshi, T. Tayami, and S. Tanaka, Jpn. J. Appl. Phys. **30**, 1854 (1991).
[13] T. M. Mayer, E. Chason, and A. J. Howard, J. Appl. Phys. **76**, 1633 (1994).
[14] C. C. Umbach, R. L. Headrick, and K.-C. Chang, Phys. Rev. Lett. **87**, 246104 (2001).
[15] S. Roorda *et al.*, Nucl. Instrum. Methods Phys. Res., Sect. B **106**, 80 (1995).
[16] D. M. Stein *et al.*, Rev. Sci. Instrum. **75**, 900 (2004).
[17] D. M. Stein, J. Li, and J. A. Golovchenko, Phys. Rev. Lett. **89**, 276106 (2002).
[18] Tip curvature radius: $\sim$5 nm; aspect ratio $>4/1$. Manufacturer: MikroMasch (Portland, OR, USA).
[19] Excessive TEM *e*-beam exposure opens ion-sculpted nanopores. The pore in the upper right of Fig. 4 opened while adjusting the microscope for optimal image quality.
[20] *Physics of Semiconductor Devices*, edited by S. M. Sze (Wiley, New York, 1981).